express $\mathfrak{L}_1$ in terms of the ξ_j, transforming (E2) to the form

$$\frac{d}{dt}\langle Q\rangle=\mathfrak{L}_2\left(\lambda,\lambda^*,\xi_j;\frac{\partial}{\partial\lambda},\frac{\partial}{\partial\lambda^*},\frac{\partial}{\partial\xi_j}\right)\langle Q\rangle. \quad \text{(E3)}$$

The final stage is to express $\langle Q\rangle$ as the left side of (5.5) and to reverse the procedure which led from (E1) to (E2), obtaining an equation of the form

$$\frac{d}{dt}\langle Q\rangle=\int^{(6)}\exp i(\lambda^*b+\lambda b^*+\sum\xi_jX_j)$$

$$\times\mathfrak{F}_2\left(\frac{\partial}{\partial b},\frac{\partial}{\partial b^*},\frac{\partial}{\partial X_j};b,b^*,X_j\right)P_2d^{(2)}bd^{(4)}X, \quad \text{(E4)}$$

where [see also (6.1)] we have used the notation

$$X_j(j=1,2,3,4)\equiv(N_1,N_2,M,M^*)$$

$$d^{(4)}X\equiv dN_1dN_2d(\mathrm{Re}M)d(\mathrm{Im}M).$$

In (E4), the operator $\mathfrak{F}_2$ comes out to be the complete curly bracketed Fokker–Planck operator on the right-hand side of (5.7) after all derivatives higher than the second have been discarded. Extraction of the integrand of (E4) by Fourier transform yields (5.7).

Carrying out the above procedure, we find that passage from $\mathfrak{F}_1$ to $\mathfrak{F}_2$ entails the following set of substitutions:

$$\beta\rightarrow b+\frac{1}{2}\frac{\partial}{\partial b^*},$$

$$\frac{\partial}{\partial\beta}\rightarrow\frac{\partial}{\partial b},$$

$$\mathfrak{M}\rightarrow\left[1+\frac{1}{2}\left(\frac{\partial}{\partial N_2}+\frac{\partial}{\partial N_1}\right)\right]M+\frac{1}{2}\frac{\partial}{\partial M^*}(N_1+N_2),$$

$$\frac{\partial}{\partial\mathfrak{M}}\rightarrow\frac{\partial}{\partial M}\left[1-\frac{1}{2}\left(\frac{\partial}{\partial N_2}+\frac{\partial}{\partial N_1}\right)\right],$$

$$\mathfrak{N}_j\rightarrow\left(1+\frac{\partial}{\partial N_j}\right)N_j+\frac{1}{2}\left(\frac{\partial}{\partial M}M+\frac{\partial}{\partial M^*}M^*\right),$$

$$j=1,2$$

$$\frac{\partial}{\partial\mathfrak{N}_j}\rightarrow\frac{\partial}{\partial N_j}-\frac{1}{2}\left(\frac{\partial^2}{\partial N_j^2}+\frac{\partial^2}{\partial M\partial M^*}\right)\qquad j=1,2 \quad \text{(E5)}$$

along with the conjugates of the first four. These replacements are made without disturbing the order of factors. In $\mathfrak{F}_1$, products of field quantities times atomic quantities such as $\beta^*\mathfrak{M}$ and $\beta\mathfrak{N}_1$ occur, but these give no ordering problems since their replacements commute. After the replacements, all derivatives higher than the second are discarded.

PHYSICAL REVIEW VOLUME 161, NUMBER 2 10 SEPTEMBER 1967

Paramagnetic Relaxation Measurements on Ce, Nd, and Yb in $CaWO_4$ by an Electron Spin-Echo Method

A. KIEL AND W. B. MIMS
Bell Telephone Laboratories, Murray Hill, New Jersey

(Received 13 March 1967)

Lattice relaxation measurements have been made for Ce^{3+}, Nd^{3+}, and Yb^{3+} at axial sites in $CaWO_4$ by a novel spin-echo method. In this method the spin system is inverted by adiabatic rapid passage, and the magnetization is later sampled by a two-pulse echo sequence. Temperatures were in the range from 1.4 to 9°K, the transfer of cold helium gas being used to maintain temperatures of 4.7°K and above. The relaxation behavior of all the ions appeared to be best described by a direct process ($w\propto T$) going over into a Raman process ($w\propto T^n$) in the vicinity of 4°K. The results could not, however, be fitted to the T^9 law, which arises in simple theoretical treatments of the Raman process, but yielded powers of the absolute temperature between 10 and 11. Orbach processes did not seem to be relevant. Two causes for this behavior are considered: dispersion in the phonon spectrum, and the inadequacy of an approximation which is commonly made in treating the denominator of the Raman integral. The Yb relaxation rate showed a marked angular variation in the Raman region. This is discussed in terms of a possible admixture of the two processes which, in the simple theory, lead to T^7 and T^9 laws.

I. INTRODUCTION

We have made lattice relaxation measurements for the three Kramers doublet ions Ce^{3+}, Nd^{3+}, and Yb^{3+}, in axial sites in a $CaWO_4$ lattice. The experimental frequency was 9.4 Gc/sec, and the temperature range 1.8 to 9°K. The measurements were made by a method analogous to that often used in nuclear relaxation studies, in which the spin system is inverted and its magnetization sampled after a variable time interval by means of a two-pulse spin-echo sequence. In our experiments, an adiabatic rapid passage was used rather than a 180° pulse to invert the spins, since it was virtually impossible to realize the latter pulse condition with the broad resonance lines, which we encountered in the materials studied. The relaxation behavior of all three ions appeared to be best described by a direct process going over into a Raman process above ~4°K. Although some problems arise in this interpretation, we believe that it is essentially correct,

and that the Orbach process[1] plays a negligible role in the relaxation of these ions in the range covered by our experiments.

The first section of the paper is devoted to a description of the method and to a discussion of certain specific experimental problems which arise when using it. Some general comments have been added regarding the relative usefulness and applicability of the method, in the hope that these may be helpful to others in planning similar experiments. The experiments on the three rare-earth ions are described in detail in the second section, and a discussion of the results follows in the third section.

II. THE MEASUREMENT OF LATTICE RELAXATION TIMES BY FAST PASSAGE AND ELECTON SPIN ECHOES

A. Microwave Pulses and the Measurement of Magnetization

The spin-echo apparatus itself has been described elsewhere,[2] and we confine ourselves to noting its principal characteristics. Two microwave pulses, each 0.2 μsec long, are generated in succession by a fixed frequency klystron and are fed to a cavity with a $Q\sim1500$. The available power of 50 W is more than ample since 1 W (giving an rf field $H_1\sim\frac{1}{2}$ G at the sample) is sufficient, at $g=2$, for both the rapid passage and the generation of echoes. The echo pulses are detected in a superheterodyne system with an i.f. of 60 Mc/sec, rectified by a second detector crystal, and applied to a boxcar circuit which gives a dc level proportional to the height of the echo.

Figure 1 shows the timing relations between the field sweep and the microwave pulses. The two-pulse spin-echo sequence samples portions of the inhomogeneous resonance line, $\sim$1 G wide, in the manner described in Ref. 2. The adiabatic rapid passage inverts the whole of the line, and is brought about by applying a 20-μsec

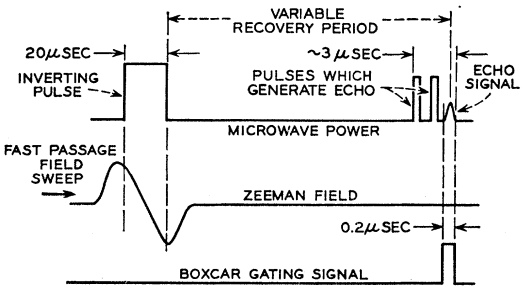

FIG. 1. Timing diagram for pulses and waveforms used in the measurement of lattice relaxation. The field sweep and the larger microwave pulse invert the spin system by means of an adiabatic fast passage. The two short microwave pulses give rise to an electron spin-echo signal which measures the magnetization of the spin system at some time during its return to the normal Boltzmann equilibrium. The boxcar gating signal enables one to select the spin echos from the other microwave pulses.

[1] R. Orbach, Proc. Roy. Soc. (London) **264**, 458 (1961).
[2] W. B. Mims, Rev. Sci. Instr. **36**, 1472 (1965).

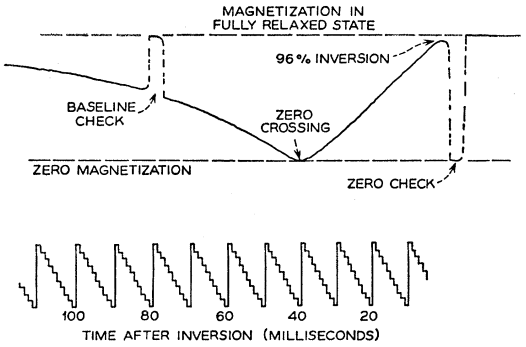

FIG. 2. Typical recorder tracing, showing the recovery towards Boltzmann equilibrium after the magnetization has been inverted by an adiabatic fast passage. This tracing is derived from $\sim$1000 cycles of the type shown in Fig. 1, the recovery period in each cycle being gradually lengthened as indicated on the staircase waveform below. The apparatus is not sensitive to the sign of the magnetization; hence the reversal of slope when the recovery time $\simeq$40 msec. The baseline check was made by turning off the inverting pulse, the zero check by turning off the echo generating pulses.

X-band pumping pulse in conjunction with the field sweep. When making a relaxation measurement the interval between the short pulses remains constant at some convenient value (typically 1.5 μsec), and the time interval between the passage and the echo sequence is varied electronically. The magnetization is then measured at successively later times after the spin inversion, and the boxcar circuit delivers a voltage which traces out the recovery function on a pen recorder (Fig. 2). The staircase function shown on the parallel recorder tracing in Fig. 2 is derived from a counter which measures the time t in each pulsing cycle. The recording begins and ends with a measurement of the magnetization in the fully relaxed state, and includes a check made during the middle of the run by turning off the pumping pulse for a few cycles. A zero signal-level check, made in a similar manner by momentarily turning off one of the two pulses in the spin-echo sequence, is also shown. Since the detector responds to the absolute magnitude of the echo signal and not to its phase, the pen recorder is deflected in the same direction for inverted and for normal magnetizations. Ideally, there should therefore be an abrupt reversal of slope at the transition point between these two regions. The rounding off see in the figure is caused by the bend in the rectifying characteristic of the second diode. A correction was made for this in the analysis of the data.

B. The Field Sweep

The magnetic field sweep for the rapid passage was generated by two sets of Helmholtz coils located on either side of a silvered Pyrex cavity. The resulting field was monitored by a smaller coil, whose output was fed via an integrating amplifier to an oscilloscope. A field sweeping function of the form shown in Fig. 1 has the advantage that current flows only for a small fraction of the total time. Heating in the cryostat can

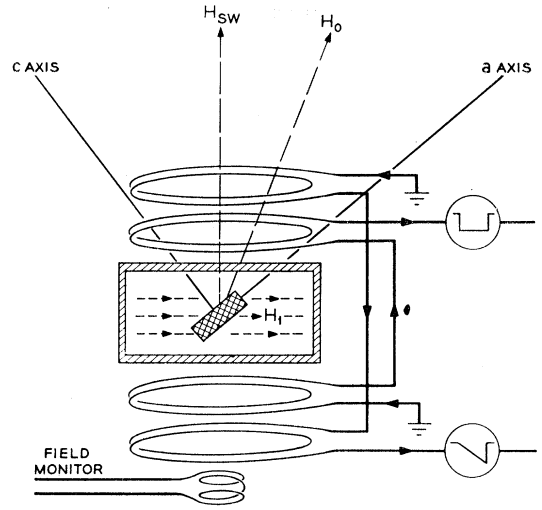

FIG. 3. Geometry of field-sweeping coils, sample, and fields in the microwave cavity. The driving circuits give negative-going current waveforms. The coils are connected in opposite senses so that these current waveforms generate a resultant sweeping field H_{sw} of the form shown in Fig. 1. The field monitor coil is connected to an integrating amplifier in order to display H_{sw}. It is possible to rotate H_0 in a 90° wc (e.g., from a-axis to c-axis alignment) without a serious loss in the efficiency of H_{sw} or in the coupling of the spin system with H_1.

be held to a minimum, and the coils can be driven by output tubes which are normally in the cutoff state. Two independent output stages were used here, each consisting of a pair of 3E29 tubes. One delivered a negative square wave and the other a negative-going ramp, the current in the ramp being adjusted to reach a peak value twice as high as the current in the square wave. These stages delivered currents of 1 and 2 A, respectively. Each was RC coupled to a separate pair of Helmholtz coils, and the connections were made in opposite senses so that the two negative-going current waveforms combine to generate the required magnetic field sweep.[3,4] (Fig. 3.)

The main practical problem in designing the sweep circuits lies in minimizing the dead time between the rapid passage and the earliest moment at which the echo pulses can be applied. This dead time depends primarily on the L/R time constant of the sweeping circuit, but it is also determined to some extent by the timing used in the echo sequence and by the width of the resonance line being studied. If, for example, the Zeeman field varies by an amount comparable with H_1 during the time τ which elapses between the first and second short pulses, then different spin packets will be excited by the two pulses, and the echo will be reduced in amplitude. This effect can only be neglected when field recovery has reached the point where the residual rate of change of field $dH_0/dt \ll H_1/\tau$. A second condition requires that, prior to the application of the short pulses, the Zeeman field should have recovered to within ΔH_0 of its resting value, where $\Delta H_0 \ll$ the linewidth. Otherwise the resonance line will initially be sampled down on one side of the peak. This will lead to a spurious rise at the beginning of the relaxation trace, as the resonance field rises to its previously adjusted value at the peak of the line. In our experiments, we found that it was usually safe to begin sampling the magnetization 40–50 μsec after the rapid passage. L/R for the sweeping circuit was 10 μsec.

C. Efficiency of the Inversion

The parameters required in order to estimate the efficiency of the inversion can readily be deduced from observations made when setting up the two-pulse spin-echo sequence. This estimate can then be used to check the observed inversion, or to indicate limits to the rate at which the field may be swept. We can define the inversion efficiency ϵ_{inv} as the ratio between the absolute magnitudes of M_z before and after the passage. ϵ_{inv} will depend on the field sweep rate dH_0/dt, on the microwave field intensity H_1, and on the phase memory of the spin packets undergoing inversion. One of the conditions for an ideal rapid passage, given by Bloch,[5] is that $T_2 \gg H_1/(dH_0/dt)$. The physical implication is as follows. During the sweep the microwave field is interacting strongly with those spin packets lying in a range $\pm H_1$ about exact resonance. It is essential, therefore, that the resonance field should move away from this portion of the line, before there has been any appreciable randomization of their phases i.e., the time $\Delta t = H_1(dt/dH_0)$ taken to traverse a portion of line H_1 wide should be an order of magnitude shorter than the dephasing time. For the purpose of applying this criterion we may take T_2 to be the observed phase memory (although this may not have a very exact meaning in an electron spin-echo experiment, since the phase memory often decays according to a function which cannot be expressed in analytic form). The magnitude of H_1 can be estimated from the behavior of the echo signal. In our experiments, the same microwave field intensity was used for the inverting pulse and for the generating pulse. An optimum echo waveform is obtained when $\gamma H_1 t_p = 2\pi/3$ (Ref. 2). Thus, if $t_p = 0.2$ μsec, $\gamma H_1 = 1.07 \times 10^7$ rad/sec, and, for the case of $g=2$, $H_1 \simeq 0.5$ G. In most of the materials studied (except at the highest temperatures) the time between pulse I and the echo corresponding to an e^{-1} reduction in echo

[3] The monitor coil was also used inside the cavity to test the penetration of the sweeping field inside the silvered cavity walls under liquid-helium conditions. An additional check on the field in the cavity was made by using the square-wave portion of the field sweep. The resonance field was measured at various times during and after the sweep by means of a two-pulse echo sequence, and the values of the sweep field were inferred from the displacements observed in the resonance.

[4] In adjusting the sweep in relation to the inverting pulse it is useful to know exactly when the sweeping field (as seen inside the cavity) passes through zero. This point is easy to find experimentally. The apparatus is first adjusted to give a spin echo from an inverted resonance line. The inverting pulse is then advanced or delayed until the echo signal falls and a sharp notch appears in the center of it. This echo waveform indicates that the inverting pulse is beginning or ending just as the sweep field crosses the resting field value H_0. Spin packets on one side of exact resonance are inverted, those on the other side are in the normal state, and interference between two oppositely directed magnetizations occurs in the echo.

[5] F. Bloch, Phys. Rev. 70, 460 (1946).

amplitude was >10 μsec. The Bloch T_2 condition therefore requires a sweep rate $dH_0/dt \gg 0.05$ G/μsec. This rate was easily exceeded in practice.

If the T_2 condition is satisfied, and H_1 and dH_0/dt are known, ϵ_{inv} can be calculated. We define a field-sweeping parameter $\sigma=\gamma H_1^2/(dH_0/dt)$. Then, for $\sigma \gtrsim 2$, $\epsilon_{\text{inv}} \simeq 1-2\exp(-\pi\sigma/2)$.[6] Let us take $\sigma=2$, giving an inversion efficiency $\epsilon_{\text{inv}}=91\%$ as a lower limit. As we have shown above, under our experimental conditions $\gamma H_1=1.07\times10^7$ rad/sec^2, and the limit therefore becomes $\gamma dH_0/dt \leq 5.5\times10^{13}$ rad/sec^2, i.e., for $g=2$ the field sweeping rate must not exceed 6.8 G/μsec, otherwise the inversion efficiency will be seriously reduced because of the passage conditions being insufficiently adiabatic.

d. Radiation Damping

For a strong sample, the radiation-damping effects which occur during the emission of the echo signal may lead to a lack of linearity in the measurements. In discussing a related problem, Bloembergen and Pound[7] represent the precessing magnetization by a single vector and assume that the resulting emf drives the resonant circuit in an approximately steady-state manner. They show that the induced field $H_i=4\pi\eta Q M_0 \sin\theta$, where η is the filling factor of the circuit, M_0 is the precessing magnetization per unit volume, and θ is the angle between M_0 and the Zeeman field. We can estimate the effect of radiation damping in our experiment by finding the ratio between the spin reorientation $\gamma H_i t_E$ which is caused by H_i operating on the spins for the duration t_E of the echo, and the angle $\gamma H_1 t_p \simeq 2\pi/3$. Setting $t_E=t_p$ and taking $\sin\theta=1$ we find that $\gamma H_i t_E/\gamma H_1 t_p = 6\eta M_0 Q \gamma t_E$. This is almost the same as the ratio t_E/τ_R, where $\tau_R=(2\pi\eta M_0 Q\gamma)^{-1}$ is the radiation-damping time constant derived by Bloembergen and Pound. In our experiments, under typical conditions, $\eta=0.01$, $g=2$, $T=4.2$°K, $Q=1000$, $H_0=3350$ G, $S'=\frac{1}{2}$, and N_0, the number of spins per unit volume *in that part of the resonance line which contributes to the echo* is 10^{17} per cc. Deducing M_0 and substituting in the above expression, we find that $\tau_R=36$ μsec., and $t_E/\tau_R=0.006$. It is not easy to see what sort of correction, linear or quadratic, in t_E/τ_R would best account for the reduction in transverse magnetization caused by the interaction of M_0 with H_i.[8] Fortunately t_E/τ_R is small, and, the high sensitivity of electron spin-echo methods make it unnecessary to use strong samples.[9] If strong interactions between the spin system and its induced radiation field should occur, they are easily noticed in an experiment, since H_i gives rise to a satellite echo appearing at an interval τ after the main echo.[10]

E. Comparison with Other Pulsed Methods

The commonly used pulsed method for determining relaxation times, in which a pumping pulse is followed by a low-level cw monitoring signal, has one major advantage: It displays the whole of a relaxation function at once. This is offset by the poor signal-to-noise ratio which results from monitoring at a low power level, and by uncertainties arising out of cross-relaxation processes, especially those processes which transfer excitation from the spin packets which are directly driven by H_1 to the remainder of the line. The cross-relaxation difficulty has been successfully overcome by Castle, Chester, and Wagner,[11] who use a fast passage to invert the whole line. An inversion could, of course, be followed by low-level cw monitoring signal or by any other means of observing the recovery of magnetization of the spin system. The advantage of spin echos over cw or various transient methods of measuring the magnetization seems to lie in the improvement which is obtainable in the signal-to-noise ratio. This results from experimental factors rather than from more fundamental considerations. One advantage lies in the use of a high value of H_1, since this gives rise to a larger precessing magnetization in the sample and hence to a larger resonance signal. Rf fields of a similar magnitude would cause saturation of the sample if the magnetization were being monitored by a cw method. It is, of course, possible to devise other types of transient experiment using a large H_1 and avoiding the problem of saturation by making a single measurement of the magnetization. In most cases however, noise from the signal source would decrease the sensitivity.[12] This problem is avoided in an echo apparatus because of the time separation between the application of H_1 and the observation of the spin signal. Using the echo method we found no difficulty in measuring the relaxation times for lines corresponding to as few as 10^{14} spins. This was useful in testing for cross-relaxation effects, and in verifying that the relaxation time of a weak impurity was not affected by the proximity of a stronger resonance line.

---

[6] This expression can be inferred from a result given by C. Zener [Proc. Roy. Soc. (London) **137**, 696 (1932)] which states that the mixing of states after an imperfect adiabatic passage is exp $(-\pi\sigma/2)$. The quantity exp $(-\pi\sigma/2)$ must be counted twice here, since we are interested in the difference between the two spin states. See also G. Wannier, Physics **1**, 251 (1965); J. M. Daniels, Can. J. Phys. **42**, 1687 (1964).

[7] N. Bloembergen and R. V. Pound, Phys. Rev. **95**, 8 (1954).

[8] The reduction in transverse magnetization can be roughly gauged by using a more elaborate pulse sequence to give an additional echo which can be made either to precede or follow the echo under study. There are, however, other complicating features which enter when strong samples are used. For example, the M_z component of magnetization in an inverted line causes the system to act as a low gain maser, giving an apparent inversion efficiency of greater than 100%. It is safer to keep the interaction between spins and radiation field weak than to attempt to correct for all these effects.

[9] Under the given experimental conditions, but with only 10^{15} spins contributing to the echo, it is possible to obtain a boxcar tracing ~60 dB above noise (Ref. 2). Little is gained by using stronger samples; signal-to-noise does not improve since it is then limited by mechanical vibration, pulse jitter, etc.

[10] K. D. Bowers and J. P. Gordon, Phys. Rev. Letters **1**, 368 (1958).

[11] J. G. Castle, P. F. Chester, and P. E. Wagner, Phys. Rev. **119**, 953 (1960).

[12] G. Feher [Bell System Tech. J. **36**, 449 (1957)] suggests 10 mW as the limit on the power which can usefully be employed when the detector is exposed to the rf signal source.

TABLE I. Direct-process relaxation parameters for Ce^{3+}, Nd^{3+}, and Yb^{3+} at axial sites in $CaWO_4$. The rates for H_0 along a and b axes are equal but the rate may vary as H_0 is rotated in the ab plane. (See Fig. 5.) Resonance frequency = 9.41 Gc/sec.

	Ce	Nd	Yb
Direct-process rate constants with H_0 along c axis (sec^{-1} deg^{-1}).	0.14	2.3	8.1
Direct-process rate constant with H_0 along a axis (sec^{-1} deg^{-1})	0.25	0.23[a]	1.6
Approximate temperature at which Raman and direct processes contribute equally when H_0 is along c axis.	3.3°K	4.2°K	4.0°K

[a] N. E. Kask has recently published curves of relaxation time versus frequency for Nd^{3+} in $CaWO_4$ at a concentration similar to ours (N. E. Kask. Fiz. Tverd. Tela **8**, 1130 (1966) [English transl.: Soviet Phys.—Solid State **8**, 900 (1966)]. At $T = 1.8$°K and a frequency of about 9.8 Gc/sec with H_0 in the ab plane, he gets $T_1 \simeq 2.4$ sec, i.e. $(TT_1)^{-1} \simeq 0.23$.

III. OTHER EXPERIMENTAL INFORMATION. RESULTS

The concentrations of rare-earth ions in the three samples studied were as follows: in (Ca, Ce)WO_4, Ce/Ca = 0.003%, in (Ca, Nd)WO_4, Nd/Ca = 0.008%, and in (Ca, Yb)WO_4, Yb/Ca = 0.004%. Na^+ ions were added to the melt in growing all of these samples, and no strong lines were observed in addition to the axial resonance spectra of the ions concerned. Samples were $\simeq$0.06 cc in volume, and were oriented on the bottom of a TE_{101} cavity as shown in Fig. 3. By setting the crystal a and c axes at 45° to the sweeping field, it was possible to rotate the Zeeman field in an arc between 0° and 90° to the c axis, without running into the condition of weak interaction with H_1, and without reaching an orientation in which the sweeping field became ineffective.[13]

At the lower end of the temperature range the relaxation rate was proportional to T, indicating that the relaxation was taking place by way of the one-phonon "direct process." Above this range, the relaxation rate increased rapidly with temperature in such a manner as to indicate a Raman process. (The evidence for this will be given in subsequent paragraphs.) The results obtained in this low-temperature range are given in Table I. In general only the relaxation rate with H_0 along the c axis and the relaxation rate with H_0 along the a axis were measured, but in one case, that of (Ca, Nd)WO_4 in the direct-process region, a complete study of the angular variation was made. It is shown in Appendix I that the angular dependence for the direct-process relaxation rate, operating between the two levels of the Kramers doublet, is given by an expression of the form

$$g^4 w = Q_{pqrs}\xi_p\xi_q\xi_r\xi_s, \tag{1}$$

where w is the relaxation rate constant, ξ are the direction cosines of the vector defining the orientation of the Zeeman field, and where the experimental microwave frequency is assumed to be constant. Q_{pqrs} is a fourth-rank tensor, symmetric under interchange of the indices, whose elements are restricted according to the point symmetry of the ion being investigated.[11] In the special case of S_4 point symmetry there are, in all, five independent parameters[15] in the terms of which the angular variations in ac, bc, and ab planes may be written

$$W_{ac} = WS = (1/g)^4\{W_1\cos^4\theta + W_2\cos^2\theta\sin^2\theta + W_3\sin^4\theta\}, \tag{2a}$$

$$W_{ab} = (1/g_\perp)^4\{W_3(\cos^4\phi + \sin^4\phi) + W_4\cos^2\phi\sin^2\phi + W_5\cos\phi\sin\phi(\cos^2\phi - \sin^2\phi)\}, \tag{2b}$$

where θ is the angle between H_0 and the c axis and ϕ is the angle between the a axis and the projection of H_0 in the ab plane. Within our experimental error of ±5% it was not possible to distinguish between Eq. (2a) and the simpler expression

$$W_{ac} = (1/g)^4\{(W_1)^{1/2}\cos^2\theta + (W_3)^{1/2}\sin^2\theta\}^2, \tag{3}$$

which can be derived from the rate constants given for Nd in Table I. The ab plane variation is shown graphically in Fig. 4. It may be noted that the varia-

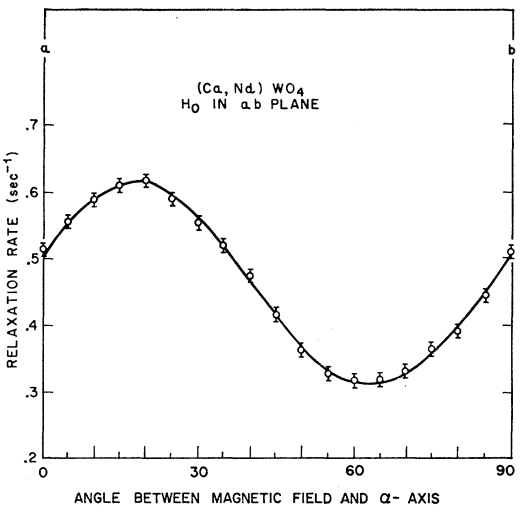

FIG. 4. Direct-process relaxation for (Ca, Nd)WO_4 as H_0 is rotated in the ab plane, $T = 2.2$°K.

[13] At the ends of the range indicated in Fig. 3, sweeping field has a component $H_{sw}/\sqrt{2}$ parallel to the Zeeman field, and at the same time causes a rotation of the Zeeman field by an angle $H_{sw}/\sqrt{2}H_0$. At 0° or 90° to the c axis only the parallel component is effective in changing the resonant frequency of the spins. Elsewhere, the parallel component and the rotation combine to produce a sweep which may be greater than or less than that due to either component alone. The contribution due to rotation can be significant for ions such as Yb^{3+} which have a large g anisotropy.

[14] See, for example, C. E. Smith [Solid State Phys. **6**, 237 (1960)] where the tensors are given in Voigt notation.

[15] The S_4 tensor given by Smith has ten coefficients. In our case, however, it is at once clear from the property of symmetry under interchange of the indices that 45 = 0, 16 = 61, and 13 = 31. Further examination shows that 44 describes the same direction cosine product as 13, and 66 the same product as 12, thus reducing the number of independent parameters to five.

tion in this plane is 2:1, whereas the variation in the *ac* plane is 10:1.

In the temperature range above 4.2°K, the sample was cooled by continuously transferring cold helium gas from the storage Dewar. The arrangement is shown diagrammatically in Fig. 5. The transfer tube was jacketed with a liquid-nitrogen bath to minimize the heat leak into the cold gas, which constitutes the chief limiting factor when approaching 4.2°K from above.[16] Our lowest temperature of 4.75°K required a consumption of liquid helium of $3\frac{1}{2}$ liters/h. There was no advantage in attempting to boil off helium at a faster rate, since at this point turbulence in the experimental Dewar caused an actual reduction in the cooling effect. Fortunately, it was only necessary to maintain this rate of helium consumption for a few minutes at a time when measuring a relaxation at the bottom of the gas transfer range. At temperatures above 6°K, the method proved to be comparatively economical (e.g., 0.5 liters/h of liquid at 6.4°K, and 0.1 liters/h of liquid at 7.4°K). Very low rates were adequate to maintain temperatures of 8°K and above. However, we found it desirable to boil off at least 0.05 liters/h. (heating the transferred gas if necessary) in order to create sufficient turbulence to maintain a uniform temperature at the bottom of the experimental Dewar. We encountered no difficulty in holding the system at the required temperature, or in going back and repeating a measurement at a particular point.

Temperatures in the range above 4.2°K were measured with a resistance thermometer, and are estimated to be within 1% of the values plotted in Figs. 6–8. In

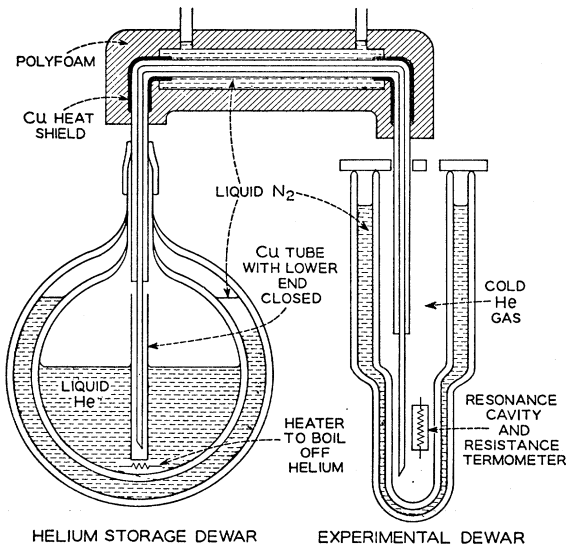

FIG. 5. Arrangement for transferring cold helium gas into the experimental Dewar. The copper tube with closed off lower end prevents the transfer of liquid. The rate of gas transfer is controlled by boiling off liquid in the storage Dewar. Temperatures down to 4.75°K were reached in the experimental Dewar.

[16] The transfer tube was especially constructed by Hofman Laboratories of Newark, New Jersey.

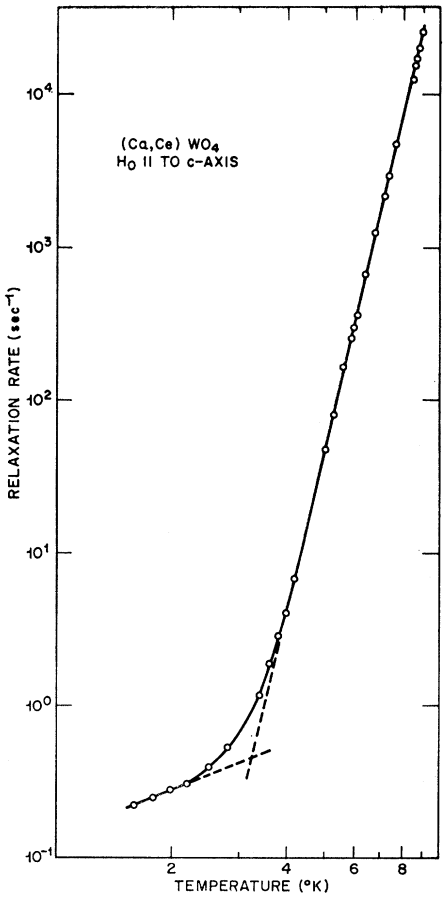

FIG. 6. Relaxation rates for (Ca, Ce)WO_4 with H_0 || to c axis. In the Raman region $w \propto T^n$, where $n=10.9\pm0.2$.

each case the relaxation rates could be fitted with a function of the form $w=AT+BT^n$. The Raman component could not, however, be made to fit the commonly assumed "T^9 law." Instead, we obtained the powers $n=10.9\pm0.2$ for Ce, $n=10.4\pm0.2$ for Nd, and $n=10.1\pm0.2$ for Yb. We were not able to fit the function $w=AT+B\exp(-\Theta/T)$ as had been our expectation.[17] Also, somewhat unexpectedly, we observed angular variations of the relaxation rate at temperatures which were well up in the Raman range. The largest was for Yb which gave a ratio of relaxation rates $w(c \text{ axis})/w(a \text{ axis})=2.0$ at 7°K. We followed the variation carefully as a function of angle in the *ac* plane and were not able to detect any sudden changes

[17] Early experiments appeared to give a reasonable degree of success in fitting this expression, and it was not until we were able to extend our measurements over several decades, that we became certain that we had a Raman process. Over a limited experimental range it may be comparatively difficult to distinguish between Raman and Orbach processes. If, for example, we plot log w against $1/T$ (without, however, knowing where to place the abscissa), it may be possible to fit the expression log $w=\log B+\Theta/T$ with the data, even when log $w=\log B+n \log T$ would be the correct form of the function. In the vicinity of $\Theta=nT$ the gradients of the two functions are approximately the same, and a variation of $\pm25\%$ in T will only lead to a difference of $\pm2\%$ in log w. If a "fit" of this kind is made, we find a value $\Theta\simeq n$ times the mean temperature of the range.

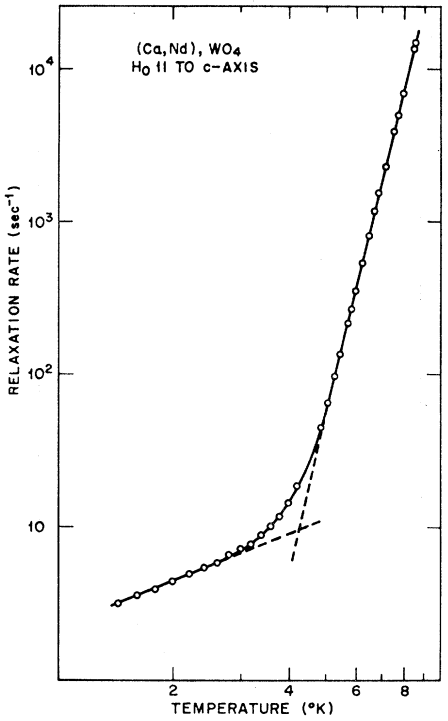

FIG. 7. Relaxation rates for (Ca, Nd)WO_4 with H_0 || to c axis. In the Raman region $w \propto T^n$, where $n=10.4\pm0.2$.

such as might have been caused by cross relaxation to an impurity.[18] Nd at 6.9°K showed a small variation, $w(c \text{ axis})/w(a \text{ axis})=0.93$, which lay barely outside the limits of our experimental accuracy. No angular variation could be detected for Ce in the Raman range.

In a paramagnetic relaxation study there are, of course, many experimental parameters which might be varied and many checks which could be made at each stage. We have not attempted to be exhaustive, but have followed our instinct in this matter. Numerous tests were made on the Nd relaxation traces to try to detect possible deviations from exponentiality. No such evidence was found. On all occasions the magnetization appeared to be relaxing according to a single exponential function from the inverted state to the position of normal temperature equilibrium. The spectra of Nd and Yb both contain numerous hyperfine lines. These were occasionally checked to see if they gave the same relaxation behavior as the main line. No significant differences were noticed. Since the field sweep was not wide enough to cover the main line as well as the hyperfine line, only the hyperfine line was inverted. The absence of any symptoms of accelerated relaxation in this line indicates that cross relaxation between lines played a negligible part in these experiments.

[18] The spectrum of the sample showed no such impurity in any case. Cross relaxation within the resonance line is ruled out on account of the experimental method used here.

IV. DISCUSSION

Perhaps the most striking feature of the results is the clear evidence for a temperature dependence faster than T^9. If the relaxation rate in the high-temperature region ($T>4.5$°K) is fitted to a T^n law, then for all three ions $n>10$. In situations such as this one might at first suspect an Orbach process in the upper part of the range. Although our results cannot be explained by a pure Orbach process, it would be possible, within the limits of experimental error, to fit the data with a mixture of Raman and Orbach processes. In fact, we believe that any significant contribution by the Orbach process can be discounted in the temperature range of interest. Consider for example Yb^{3+} where the lowest excited state[19,20] is 115 cm^{-1} above the ground state. The Orbach transition rate is given by

$$w \simeq w_0 \exp(-\Delta E/kT). \quad (4)$$

At 8°K, the exponential factor for $\Delta E=115$ cm^{-1} is 10^{-9}, so that for the Orbach process to contribute significantly, $w_0 \geq 3\times10^{13}$ sec^{-1}. This is far greater than the values of w_0 previously obtained in rare earths[21] and indeed would lead to linewidths in fluorescence of

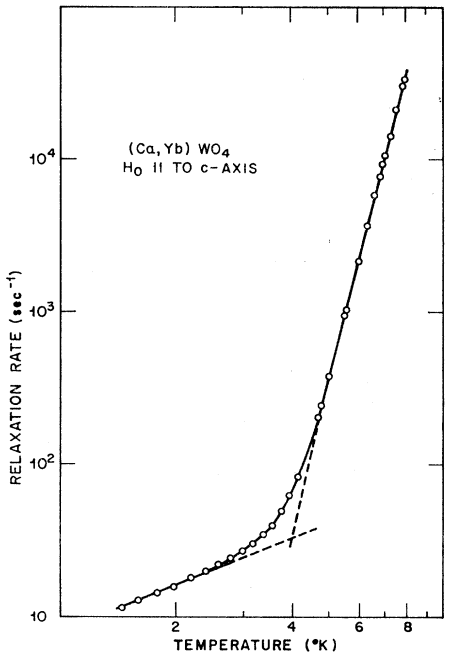

FIG. 8. Relaxation rates for (Ca, Yb)WO_4 with H_0 || to c axis. In the Raman region $w \propto T^n$, where $n=10.1\pm0.2$.

[19] D. L. Wood (private communication); G. R. Jones, Bull. Am. Phys. **11**, 812 (1966). Previously reported results (Ref. 20) assigned the lowest excited state of Yb^{3+} in $CaWO_4$ at 220 cm^{-1}. It now appears that this was probably a phonon-assisted transition.

[20] R. Pappalardo and D. L. Wood, J. Mol. Spectry. **10**, 81 (1963).

[21] G. H. Larson and C. D. Jeffries, Phys. Rev. **141**, 461 (1966); P. L. Scott and C. D. Jeffries, *ibid.* **127**, 32 (1962); R. C. Mikkelson and H. J. Stapleton, *ibid.* **140**, A1968 (1965).

about 300 cm^{-1} which are, of course, not observed. Finally we may point out that in Ce^{3+} in $CaWO_4$ there is evidence[22–24] that the lowest excited state is about 200 cm^{-1} above the ground state. In this case there is no possibility of an Orbach contribution and yet here the exponent in T^n was the greatest ($n\simeq 11$).

It seems clear that one must look for some other process to account for the observed temperature independence. In the following analysis it is not our intention to compute the magnitudes of the Raman relaxation rates. We shall demonstrate only that it is naive to expect a Raman process will give a good fit to a T^9 law in the case of rare earths above 4°K.

The electron-phonon interaction may be written as

$$\mathcal{H}_{ep}=\sum_i V_i\epsilon_i+\sum_{ij} V_{ij}'\epsilon_i\epsilon_j, \tag{5}$$

where V, V' are the appropriate potentials in the electron coordinates and the ϵ are the strains inducing these potentials. From perturbation theory it can be shown that the Raman relaxation can arise in two ways, leading to relaxation rates

$$R_1\simeq(1/\hbar^2)\rho(\nu)\rho(\nu')\mid\langle n\mid V\mid m\rangle\langle m\mid V\mid n'\rangle\mid^2\mid\epsilon_i\epsilon_j\mid^2 \tag{6a}$$

and

$$R_2\simeq(1/\hbar^2)\rho(\nu)\rho(\nu')\mid\langle n\mid V'\mid n'\rangle\mid^2\mid\epsilon_i\epsilon_j\mid^2, \tag{6b}$$

where R_2 involves only the second term on the right of Eq. (5) and R_1 is second order in the first term. In the case of non-Kramers doublets, both relaxation terms are important and there is little direct evidence indicating which of these dominates. In the present cases (all Kramers doublets), the R_2 term will lead to zero transition probability unless mixing due to a magnetic field (which lifts the Kramers degeneracy) is taken into account. For this reason, the R_2 term is usually neglected in Kramers salts. We shall, however, look into this more carefully as a possible source of the angular variation of the relaxation times observed in Yb^{3+} at 7°K.

The R_1 relaxation term may be written as[25]

$$R_1=\frac{\mid V_1V_1\mid^2\hbar^2}{\rho^2}\left(\frac{2}{a}\right)^9 v^{-1}$$

$$\times\int_0^{\pi/2}\frac{K^8\exp(-x(K))dK}{[1-\exp(-x(K))]^2[E^2-(kTx(K))^2]^2}, \tag{7}$$

where $x(K)=(\hbar/kT)\omega(K)\simeq(\hbar\omega_0/kT)\sin K$; $\omega_0=\pi v/a$ with v equal to the sound velocity and a is approximately the lattice spacing. ρ is the density of the crystal; V_1 and V_2 are the matrix elements of the potential terms associated with ϵ_1 and ϵ_2. In this expression, the effects of the finite phonon spectrum are taken into account through the simple dispersion law $\omega=\omega_0\sin(qa/2)$ (q is the wave vector). The energy denominator within the integral derives from the quantity $(\hbar\omega)^4/[E^2-(\hbar\omega)^2]^2$ and is usually approximated by $(\hbar\omega/E)^4$, where E is the energy separation to the excited state and $\hbar\omega$ is the phonon energy. The analogous expression for R_2 is

$$R_2=\frac{\mid V'\mid^2(2g'\beta H)^2}{\rho^2E^2}\left(\frac{2}{a}\right)^9\frac{1}{v\omega_0^2}$$

$$\times\int_0^{\pi/2}\frac{K^8}{\sin^2K}\frac{\exp[-(\hbar\omega_0/kT)\sin K]dK}{(1-\exp[-(\hbar\omega_0/kT)\sin K])^2}. \tag{8}$$

The simple dispersion law used in Eqs. (7) and (8) is by no means exact. However it may be expected to demonstrate the major effects of dispersion in the temperature dependence. Our treatment of this differs only slightly from that of Vredevoe[2] which was applied to a somewhat different case.

That both the dispersion curve and the *exact* energy denominator in Eq. (7) may have an important influence on the temperature dependence may be seen from the following simple considerations. In the (nominally) T^9 type of relaxation one can show that the major contribution to the integral comes from phonons with energies about ten to twenty times kT. If $20T/\Theta_D$ (Θ_D is the Debye temperature) is greater than 0.5, one can expect the approximation $\omega=\omega_0\sin K\simeq\omega_0K$ to break down. For $T=8$°K, $20T=160$°K which is as large or larger than Θ_D in most rare-earth crystals. A second consequence of the fact that the major phonon contribution occur for $\hbar\omega>10kT$ is that the energy denominator $[E^2-(\hbar\omega)^2]^2$ will often be significantly reduced even in the 4–8°K region for rare earths where E is rarely more than a few hundred wave numbers. The dispersion contribution may be expected to cause a marked increase in the temperature dependence as $20kT$ approaches Θ_D followed by a decrease toward a T^2 law for very high temperatures $T\gg\Theta_D$.

The frequency-dependent energy denominator does not occur in the R_2 expression [Eq. (8)] and the dispersion form is qualitatively different. Solutions of the integrals in (7) and (8) have been obtained numerically on a computer and are given in Figs. 9–11. The actual forms of the relaxation rate versus temperature cannot be expressed analytically. If the results are forcibly fitted to a single T^n curve, the magnitude of the best-fit value of n will depend on the maximum and minimum values of temperature in the range considered. If we set $\hbar\omega_0/k\equiv\Theta_D=140$°K, we get reasonable agreement with the relaxation data of Figs. 9–11. This value of Θ_D is not unreasonable for soft crystals such as tungstates. An example for the case of Ce, $\Delta Ek=300$°K,

[22] Using crystal-field parameters which give a rough fit to the ground-state splitting in Nd^{3+} (Ref. 24) we find that the Ce^{3+} states are at 220 and 305 cm^{-1}.

[23] L. F. Johnson and R. A. Thomas, Phys. Rev. **131**, 2038, (1963); J. G. Gualtieri and T. R. AuCoin, J. Chem. Phys. **45**, 4348 (1966).

[24] R. C. Mikkelson and H. J. Stapleton, Phys. Rev. **140**, A1968 (1965).

[25] Lawrence E. Vredevoe, Phys. Rev. **153**, 312 (1967).

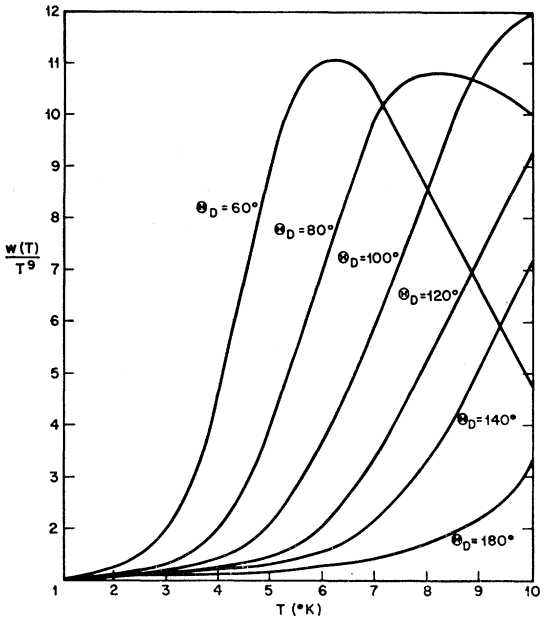

FIG. 9. Normalized Raman integral R_1 divided by T^9 versus temperature for several values of Θ_D. Only the low-temperature region is shown. The frequency-dependent part of the energy denominator in Eq. (7) has been eliminated to display the effects of dispersion alone. Without dispersion, those curves would be horizontal lines with ordinate equal to unity at the lower temperatures.

is shown in Fig. 12. The Yb^{3+} case is more complex and we will consider this further when analyzing the angular dependence of the Raman process in that case.

It may be asked why this type of temperature dependence has not been observed previsouly. Probably this is because relatively little data has been obtained for temperatures between 4.2 and 10°K and very rarely do the measurements[26] extend over several decades in relaxation time in the Raman region as in our data. If these conditions are met, it seems unlikely that a true T^9 dependence would be observed. It would be interesting to know the relaxation behavior above 4.2°K for some of the systems which have been studied in the liquid-helium range, particularly for salts with low Debye temperatures.

Another surprising feature of the experimental results was the clear-cut evidence of an angular dependence of the relaxation rate for Yb^{3+} at 7°K. At this temperature contributions from the direct process were negligible. On the other hand, there are no magnetic field terms in the expression for R_1 [Eq. (7)]. In fact, if one omits magnetic splitting of the excited states, a straightforward (but quite lengthy) computation will show that there is complete cancellation of the magnetic field terms. Direct mixing of states by the magnetic field has absolutely no effect on the Raman relaxation R_1.

[26] See, however, R. W. Bierig, M. J. Weber, and S. I. Warshaw, Phys. Rev. **134**, 1504 (1964). In this work temperatures well above 4°K were attained. However, the range of relaxation times over the Raman region was never as much as one decade.

Only a splitting of the excited state can cause this quantity to depend on the magnitude and orientation of the magnetic field. The expression for the Raman relaxation will then have the additional term

$$R_1' = \frac{|V_1V_2|^2\hbar^2}{\rho^2}\left(\frac{2}{a}\right)^9\left(\frac{g_e\beta H_z}{E}\right)^2 \times v^{-1}\int_0^{\pi/2}\frac{K^8}{\sin^2 K}\frac{\exp(-x(K))dK}{[1-\exp(-x(K))]^2[E^2-(kTx(K))^2]^2}, \quad (9)$$

where all quantities are the same as in Eq. (7) and g_e is the g value of the excited state in a given direction. Note that the integral leads to the nominal T^7 type of temperature dependence. At low temperatures (i.e., neglecting dispersion and the energy denominator), we find that for our case (the Yb^{3+} ground manifold[19] is shown in Fig. 13)

$$\frac{R_1'}{R_1}\simeq\frac{1}{7.8}\left(\frac{g_e\beta H_z}{kT}\right)^2\simeq\frac{1}{7.8}\times\left(\frac{2°}{7°}\right)^2.$$

This ratio is far too small to account for the variation in relaxation time. This effect will generally be negligible unless $(g_e\beta H)_{\max}\geq 4kT$, which will rarely be realized in a region where the Raman process dominates.

The remaining obvious possibility for explaining the angular dependence observed is then the R_2 process. We do not have sufficient information to calculate R_2/R_1 since the magnitudes of V' and the V are unknown. It may be of some interest, however, to consider the ratio of R_2 and R_1 for Yb under idealized conditions. From Eqs. (7) and (8)

$$R_2/R_1=\frac{|V'|^2}{|V_1V_2|^2}\frac{E^4}{(E')^2}\left(\frac{2g'\beta H}{kT}\right)^2\frac{\alpha}{7.8},$$

where E' takes into account the fact that R_2 and R_1

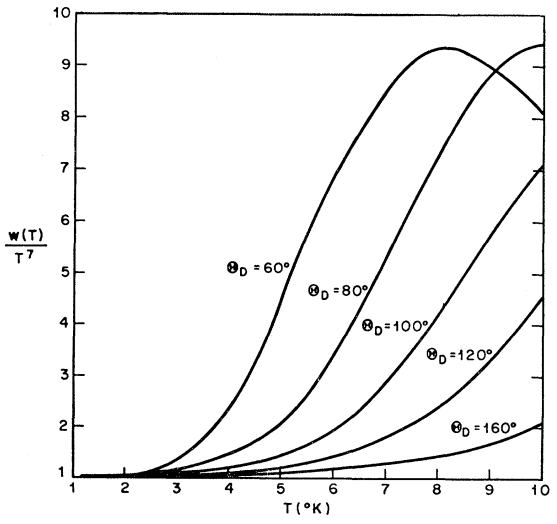

FIG. 10. Normalized Raman integral R_2 [Eq. (8)] divided by T^7 versus temperature for several values of Θ_D.

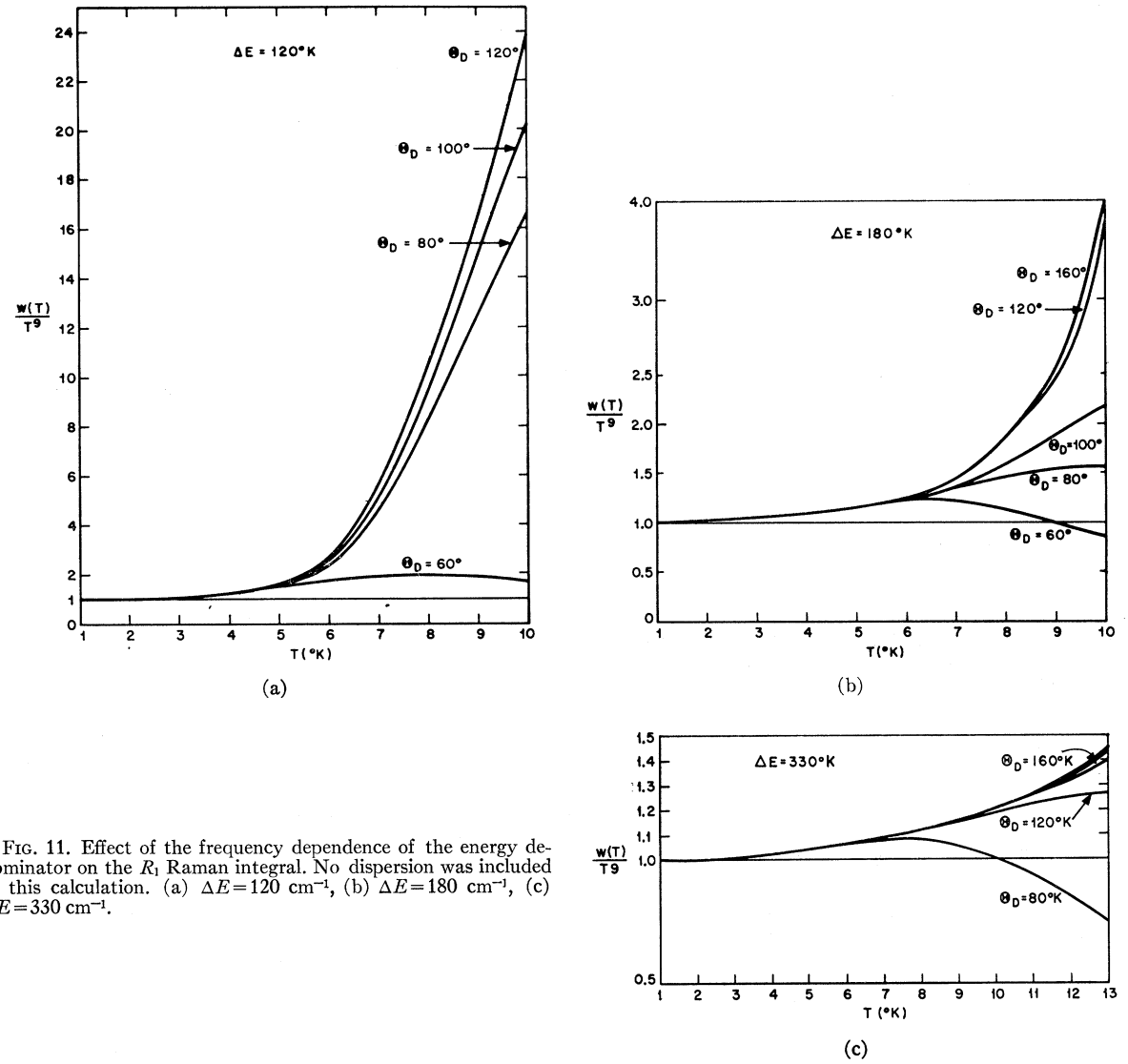

FIG. 11. Effect of the frequency dependence of the energy denominator on the R_1 Raman integral. No dispersion was included in this calculation. (a) $\Delta E=120$ cm^{-1}, (b) $\Delta E=180$ cm^{-1}, (c) $\Delta E=330$ cm^{-1}.

may involve different electronic intermediate states. g' is an effective off-diagonal g component and α takes into account the relative effects of dispersion and the energy denominator. At X band and for H perpendicular to the c axis, the ground state will mix primarily with the lowest excited state at 115 cm^{-1}, giving $2g'\beta H_x/k=0.65$°K. Setting $E=E'$, $\alpha=1$ we get at $T=7$°K, $R_2/R_1=4.1\times10^{-5}\,|\,V'\,|^2E^2/\,|\,V_1V_2\,|^2$. If R_1 and R_2 involve mixing of the ground state with the same excited level, we must take account of correlations between the relevent off-diagonal elements. Assuming destructive interference, a ratio of R_2/R_1 as small as 0.05 would be adequate to explain our result. Then $|\,V'\,|^2E^2/\,|\,V_1V_2\,|^2=1.3\times10^4\,|\,V'\,|^2/\,|\,V_1V_2\,|^2>1200$. Similarly for H parallel to c we find $2g'\beta H_z=1.37$ cm^{-1}, $E'=115$ cm^{-1}, and

$$R_2/R_1=2.5\times10^{-4}\,|\,V'\,|^2E^2/\,|\,V_1V_2\,|^2.$$

For the same conditions as above (we need constructive interference in this case, however), the requirement on $|\,V'\,|^2E^2/\,|\,V_1V_2\,|^2$ is still about the same, $1.3\times10^4\,|\,V'\,|^2/\,|\,V_1V_2\,|^2>400$. It is not possible to judge conclusively whether these conditions can actually be satisfied, i.e., that V' in Eq. (11) is at least 20 times greater than V.[27] Some moderately plausible support for this model may be gained by noting that the temperature dependence of Yb in this range is somewhat slower than either Nd^{3+} or Ce^{3+}. Furthermore, the magnetic interaction of the Yb ground state

[27] From Fig. 10 it can be seen that it is possible for a pure magnetic (R_2 type) process to exhibit a T^{10} dependence in this temperature range. That is, for $\Theta\simeq80$°K, there is an increase of the integral due to dispersion of almost a factor of 8 between 4 and 8°K. This would promote a T^7 to an approximate T^{10}. However this seems unlikely since the Ce and Nd data would be very poorly fitted by so low a Θ_D and the necessary ratio of $|\,V'\,|/|\,V_1\,|$ would have to be greater than 100.

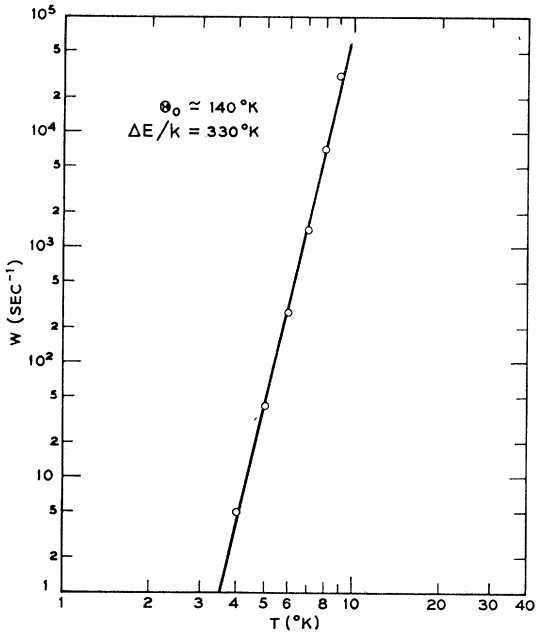

FIG. 12. Normalized Raman relaxation of Ce^{3+} versus temperature. ΔE is taken as 220 cm^{-1} and $\Theta_D = 140$ cm^{-1}. The scale used is the same as in Fig. 6. The solid line is a reproduction of Fig. 6 between 4 and 9°K.

with its excited states is rather large. However, considerably more work is required to establish definitively the nature of this orientation dependence of the Raman relaxation in Yb^{3+}.

In Table I, the direct-process relaxation times along the c axis and a axis are given. A derivation of the relation between the relaxation rate and magnetomechanical tensor is given in the Appendix for some special cases and the forms of the angular dependence are demonstrated there. However we would like to point out that some general features of the direct process, concerning relative magnitudes for different ions and relative angular dependence may be obtained from the state functions and energy levels alone.

In Ce^{3+}, the ground state is $0.89\,|\,\frac{5}{2},\pm\frac{5}{2}\rangle+0.45\,|\,\frac{5}{2},\pm\frac{3}{2}\rangle$ with $g_{||}=2.93$ and $g_\perp=1.43$. The separation between this state and the $|\,\frac{5}{2},\pm\frac{1}{2}\rangle$ state is about 230 cm^{-1} and from the ground state to the next state 305 cm^{-1}. Let us define the magnetic coupling ratios at X band as

$$\eta_{||}=2\langle e\,|\,\beta H_z(L_z+2S_z)\,|\,g\rangle/\Delta E$$

and

$$\eta_\perp=2\langle e'\,|\,\beta H_\perp(L_x+2S_x)\,|\,g\rangle/\Delta E',$$

where g denotes the ground state, e and e' are excited states, and ΔE and $\Delta E'$ are the energy separations. The coupling ratios for Ce are $\eta_{||}=9\times10^{-4}$ and $\eta_\perp=8.9\times10^{-4}$. This compares with $\eta_{||}=4.1\times10^{-3}$ and $\eta_\perp=1.9\times10^{-3}$ for Yb^{3+}. For Nd^{3+}, the ground state is $0.64\,|\,\frac{9}{2},\frac{9}{2}\rangle+0.63\,|\,\frac{9}{2},\frac{1}{2}\rangle+0.44\,|\,\frac{9}{2},-\frac{7}{2}\rangle$ and the nearest

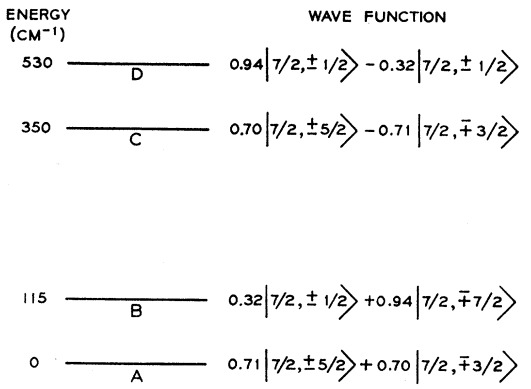

FIG. 13. Ground-state energy levels and wave functions of Yb^{3+} in $CaWO_4$.

state[23] at about 115 cm^{-1} is of the same[28] representation, $0.47\,|\,\frac{9}{2},\frac{9}{2}\rangle+0.17\,|\,\frac{9}{2},\frac{1}{2}\rangle-0.86\,|\,\frac{9}{2},-\frac{7}{2}\rangle$. The magnetic coupling ratio in this case is (for H parallel), $\eta_{||}=4\times10^{-3}$. For H perpendicular, the state $0.53\,|\,\frac{9}{2},\frac{5}{2}\rangle+0.85\,|\,\frac{9}{2},-\frac{7}{2}\rangle$ with energy 270 cm^{-1} couples strongest. $\eta_\perp$ in this case equals 6×10^{-4}. Since the magnetic coupling enters as $(g'\beta H/E)^2$ we can easily see the qualitative differences in the relaxation times for these ions.

More specifically, referring to Table I, we can see that the relaxation rate for H parallel is much larger than for H perpendicular for Nd and Yb in agreement with the magnetic mixing estimates above; for Ce where the mixing ratio is about equal for the two directions, the difference in relaxation rates is rather smaller than for the other cases; and finally that the relaxation times comparisons for different ions follow roughly the mixing ratios calculated.

We can compare the results given in Table I with Eq. (A5) of the Appendix. We find that the ratios of relaxation rates for **H** along a to those with **H** along c agree qualitatively with Eq. (A5) for Ce and Yb with $T_{xz}{}^{xz}\cong1.4T_{xy}{}^{xy}$ in the former case and $T_{xz}{}^{xz}=0.19T_{xy}{}^{x}$ in the latter. Nd does not agree with Eq. (A5) (the perpendicular relaxation rate is about 50% too small to be fitted by this equation). It is probable that the expression for full S_4 symmetry is required.

APPENDIX A

In the principal axis system of an $S'=\frac{1}{2}$ ion, we can write the static spin-Hamiltonian as

$$\mathcal{H}_0=\sum_m g_m\beta H_m S_m. \qquad \text{(A1)}$$

The relaxation interaction for the direct process may be expressed in terms of the magnetomechanical fourth-

[28] In Ref. 23, the representation of the first excited state of the $^4I_{9/2}$ of Nd in $CaWO_4$ is quoted as being opposite to what we have assumed. However, the selection rules based on this identification are ambiguous and theoretically our choice seems more likely.

rank tensor $T_{ij}{}^{kl}$ as

$$\mathcal{H}_1=\{\epsilon^{ij}T_{ij}{}^{kl}\beta H_l S_k\}, \tag{A2}$$

where ϵ^{ij} is the strain and the curly brackets imply summation over repeated indices. Both T and ϵ are defined as dimensionless quantities.

The direct-process relaxation rate w may be expressed in a form independent of the representation

$$w=\frac{1}{\hbar^2}\frac{\mathrm{Tr}[\mathcal{H}_1,\mathcal{H}_0]^2}{\mathrm{Tr}\mathcal{H}_0{}^2}\rho(\nu). \tag{A3}$$

It is easy to show that $\mathrm{Tr}\mathcal{H}_0{}^2=\frac{1}{2}g^2\beta^2H^2$. In relaxation experiments the microwave frequency is held constant. We can therefore rewrite Eq. (A3) as

$$g^4w=-\frac{2\nu^2\rho(\nu)}{\hbar^2}\mathrm{Tr}\{\epsilon^{ij}\epsilon_{pq}T_{ij}{}^{kl}T_{pq}{}^{uv}q_mq_n\xi_l\xi_v\xi_m\xi_n \times[S_k,S_m][S_u,S_n]\},$$

where ξ_l are the direction cosines of the magnetic field. Recalling $\mathrm{Tr}S_iS_j=\frac{1}{3}S(S+1)\delta_{ij}$, we have

$$g^4w=-\frac{1}{2}\frac{\nu^2\rho(\nu)}{\hbar^2}\{\xi_l\xi_v\xi_m\xi_n\epsilon^{ij}\epsilon_{pq}[g_ng_m(1-\delta_{nm})T_{ij}{}^{nl}T_{pq}{}^{mv} -g_m{}^2\delta_{nm}(1-\delta_{kn})T_{ij}{}^{kl}T_{pq}{}^{kv}]\}$$
$$=\sum_{l,v,m,n}\xi_l\xi_v\xi_m\xi_nQ_{lvmn}. \tag{A4}$$

In this form we can see the dependence of the quantity g^4w on the four direction cosines quite clearly. Equation (A4) cannot be simplified significantly without losing generality. If we assume a cubic lattice (although the *site* symmetry need not be cubic in the following) we have $\langle\epsilon_{ii}{}^2\rangle=(\hbar/M\omega)(q^2\bar{n}/15)$, $\langle\epsilon_{ii}\epsilon_{jj}\rangle=-(1/30)(\hbar q^2\bar{n}/M\omega)$, and $(i\neq j)$, $\langle\epsilon_{ij}\epsilon_{ij}\rangle=\langle\epsilon_{ij}\epsilon_{ji}\rangle=\frac{1}{5}(q^2\hbar\bar{n}/M\omega)$, where q is the wave vector, M is the crystal mass, and n is the number operator. Using these relations, we can simplify Eq. (A4) further by summing over i, j, p, and q. As an example of the type of final result, we have for cubic site symmetry

$$w^4=\frac{\hbar\omega^5}{2\pi\rho v^5}\frac{1+e^{-h\nu/kT}}{1-e^{-h\nu/kT}} \times[\tfrac{2}{5}(n^4+l^4+m^4)(T_{xy}{}^{xy})^2+\tfrac{1}{5}(n^2l^2+n^2m^2+m^2l^2) \times(2(T_{xx}{}^{xx}-T_{xx}{}^{yy})^2+(T_{yy}{}^{xx}-T_{xx}{}^{yy})^2)],$$

where l, m, and n are the usual direction cosines, $l=\sin\theta\cos\phi$, $\cdots$.

$$g^4w=\frac{\hbar\omega^5}{2\pi\rho v^5}\frac{1-e^{-h\nu/kT}}{1+e^{-h\nu/kT}} \times\{\tfrac{1}{5}(l^4+m^4)[g_\perp{}^2(T_{xy}{}^{xy})^2+g_\perp{}^2(T_{xz}{}^{xz})^2]+\tfrac{2}{5}n^4g_{||}{}^2(T_{xz}{}^{xz})^2 +l^2m^2[g_\perp{}^2\tfrac{1}{5}(T_{xz}{}^{xz})^2+\tfrac{1}{5}g_\perp{}^2(T_{xx}{}^{xx}-T_{yy}{}^{yy})^2] +\tfrac{1}{5}(l^2n^2+m^2n^2)[g_{||}{}^2(T_{xy}{}^{xy})^2 +(g_\perp{}^2-2g_\perp g_{||})(T_{xz}{}^{xz})^2+N]\}, \tag{A5}$$

where N is a complicated collection of all the "non-shear" terms.[29]

For lower tetragonal symmetry, C_4 and S_4, the tensors in the above expression, become still more complex and an additional term, $(l^2-m^2)lm$, arises.

In general, relaxation expressions are too complex to use for determining the components of the magneto-mechanical tensor by microwave relaxation experiments. However, by choosing special orientations, the shear terms can be evaluated. For example in D_{2d} symmetry, the direct relaxation for H along c determined $T_{xz}{}^{xz}$ and using this, the relaxation time for H parallel to x or y determines $T_{xz}{}^{xz}$. Another measurement in the xy plane determines $(T_{xx}{}^{xx}-T_{xx}{}^{yy})^2$. However, the quantities occurring in N in Eq. (A5) always occur as a group and cannot be determined individually.

In the case of $CaWO_4$, the lattice had D_{4h} symmetry rather than cubic symmetry. In this case the Christoffel symbols have to be included in the lattice sums.

However, for tetragonal symmetries, these can be incorporated into the T tensor elements for the n^4, l^4, m^4, and m^2l^2 terms and in a more complicated fashion for the other terms.

[29] $N=\frac{1}{3}g_{||}g_\perp[(T_{xx}{}^{xx}-T_{xx}{}^{zz})^2+(T_{yy}{}^{xx}-T_{xx}{}^{zz})^2+(T_{zz}{}^{xx}-T_{zz}{}^{zz})^2 -(T_{xx}{}^{xx}-T_{xx}{}^{zz})(T_{zz}{}^{xx}-T_{zz}{}^{zz})-(T_{yy}{}^{xx}-T_{xx}{}^{zz})(T_{zz}{}^{xx}-T_{zz}{}^{zz}) -(T_{xx}{}^{xx}-T_{xx}{}^{zz})(T^{xx}-T_{zz}{}^{zz})]$.